Unstructured Large Eddy Simulation of the passive control of the flow in a weapon bay

V. Levasseur[a], P. Sagaut[b],*, M. Mallet[a], F. Chalot[a]

[a]*Institut Jean le Rond d'Alembert, Université Pierre et Marie Curie - Paris 6, 4 place Jussieu - case 162, 75252 Paris Cedex 05, France*
[b]*Aircraft Technical Engineering and Loads Division, Dassault-Aviation, 78, quai Marcel Dassault, 92552 Saint-Cloud, France*

Abstract

The control of cavity flows has been investigated by the means of Large Eddy Simulations. The computations have been carried out on unstructured meshes to assess the efficiency of two passive acoustic oscillation suppression devices: the rod-in-crossflow and the flat-top spoiler. Despite a sustained interest and many experiments, a clear explanation for observed reduction in the flow-induced structure load is still missing. This work explores different hypotheses: the modification of the mean field and its linear stability properties, a pure deflection effect of the separated shear layer, or scale coupling between the rod wake and the turbulent mixing layer over the cavity. The aim here is to enhance the experimental database and provide leads towards a better understanding of the phenomena. The selected test-case is a cavity of length/depth ratio equal to 5, at Mach and Reynolds number of $M_\infty = 0.85$ and $Re_L = 7.10^6$, respectively.
© 2008 Elsevier Ltd. All rights reserved.

Keywords: Large Eddy simulation; Rossiter aero–acoustic mode; Flow control; Cavity flow; Turbulence

1. Introduction

The flows over cavities are very common in both internal or external aerodynamics, and can be potentially damageable in many cases. If the flow within the recess can be described as the interaction between different well-known phenomena, such as hydrodynamic instabilities, acoustic wave propagation, and aero-acoustic coupling, an important non-linear coupling of these mechanisms occurs. Since Rossiter's (1964) works, the aero-acoustic coupling is known to induce major periodic pressure fluctuations in the case of a subsonic flow over an open cavity. This is the case we are currently interested in. Beside its academic interest, it is also a major concern for aircraft makers since large amplitude aerodynamic loads develop in an open store bay leading to structural vibrations that could endanger the integrity of the aircraft. Depending on the flight altitude, the Rossiter modes can cover a 0–150 Hz range, preventing from a structural answer to the problem. It thus appears as an important problem in an industrial context, which involves complex and still unknown mechanisms.

The aerodynamic loads inside the cavity are driven by a natural flow instability. Schematically (see Fig. 1) the vortex shedding emerging from the mixing layer impinges the downstream corner of the enclosure, arousing pressure waves. These waves go back up to the upstream corner and interact with the mixing layer. Thus, this coupling of a convectively

---

*Corresponding author.

E-mail address: pierre.sagaut@upmc.fr (P. Sagaut).

Nomenclature		n	mode number
		p_i, T_i	isentropic pressure and temperature
A_i	ith Euler Jacobian matrix	Q_n	space–time slab
f_n	Rossiter tones frequency	Re_L	Reynolds number
F, F^d	Euler and diffusive fluxes	$\mathscr{S}_n^h, \mathscr{V}_n^h$	trial and weighting function space, respectively
$K = [K_{ij}]$	diffusivity matrix		
L, W, D	cavity length, width and depth, respectively	U_∞	external flow velocity
$\mathscr{L}$	steady compressible Navier–Stokes operator	U, W	conservative variables vector and weighting function
M_∞	external Mach number	κ, γ	constants of Rossiter's formula

amplifying Kelvin–Helmholtz type shear-layer instability and pressure waves leads to a self-sustained mechanism, inducing aerodynamic loads inside the cavity, pressure drag, and white-noise in the far-field.

Rossiter (1964) proposed the following semi-empirical relation for the prediction of the frequency of the cavity tones:

$$f_n = \frac{U_\infty}{L} \frac{n - \gamma}{M_\infty + 1/\kappa}, \tag{1}$$

where U_∞ and M_∞ are the external flow velocity and Mach number, respectively, L is the length of the cavity, n is the mode number, and γ and κ are two parameters adjusted from experiments. κ is generally taken equal to 0.57 and γ is a function of the length over depth ratio L/D varying from 0 (deep cavity) to 0.57. This above mentioned formula (1) has already been widely and successfully used to predict the frequencies of tones observed in a great variety of cavity flows. Hereafter, the emerging cavity tones will hence be referred to as the Rossiter modes. Beside a very good concordance, the formula also provides an *a posteriori* interpretation of the self-sustained mechanisms based on two phenomena already mentioned: the mixing layer vortices moving downstream at a κU_∞ velocity on the one hand, and pressure waves travelling upstream at the speed of the sound with a γ phase shift on the other hand.

Many experimental studies have been devoted to cavity flows (Sarohia, 1975; Knisley and Rockwell, 1987; Gharib and Roshko, 1987; Cattafesta et al., 1997; Lin and Rockwell, 2001; Rockwell et al., 2003; Ziada et al., 2003; Oshkai et al., 2005) but they mostly deal with incompressible or low Mach number flows. An important step was made by Forestier et al. (2003) who performed experiments at high subsonic speed with not only pressure measurements but also PIV, making possible an intensive study of the mechanisms.

The first computations of cavity flows, based on the resolution of bidimensional Navier–Stokes equations with an algebraic model of the turbulence, enable to predict the Rossiter modes frequency and the mean pressure drag on the floor of the recess with a fairly good accuracy. Yet, the overall pressure levels were generally underpredicted by up to 20 dB. Advances occurred in the late 1990s by the use of hybrid turbulence models such as VLES (Sinha et al., 1998), zonal decomposition RANS/LES (Arunajatesan and Sinha, 2001) or using LES (Dubief, 2000; Avital, 2001; Gloerfelt et al., 2002; Rizzetta and Visbal, 2003; Shieh and Morris, 2000). The reader is referred to reference books for detailed descriptions of these approaches (Sagaut, 2005; Sagaut et al., 2006). The best results were provided by the LES method, which is known to be very efficient for separated flows (Manoha et al., 2000; Raverdy et al., 2003; Labbe et al., 2002). The main reasons for that efficient advanced modelling strategies have been proposed during the last decade (Terracol et al., 2001; Quemere et al., 2001; Meyers et al., 2006), which allow for an optimal use of the computational resources. After having assessed the feasibility of its LES approach by computing the flow over a deep cavity, with experimental comparisons including pressure measurements and velocity-field data, Larchevêque and coworkers (Larchevêque et al., 2003, 2004, 2007) provide very accurate results for compressible cavity flows. These authors also provide a large amount of analysis tools and methods.

The control of cavity flows has attracted a lot of interest, and experiments have followed one another since the late 1970s. Previous experiments and computations studied different suppression strategies dealing with the use of ramps, spoilers, rods, air jets, etc. Investigations also dwelt upon active control with vibrating ramps, synthetic or pulsating jets. But the design of effective feedback controller remains problematic. Cattafesta et al. (2003) made a review of active control of flow-induced cavity oscillations comparing different palliatives and describing successes and failures in reducing the pressure levels. Finally, let us note the work of Stanek et al. (2000, 2001, 2002, 2003) who studied high frequency acoustic suppression strategy, including the rod-in-crossflow and the spoiler. The authors stated that high frequency forcing modify the hydrodynamics stability properties thus explaining the oscillations suppression efficiency. In the same way, they explained that the rod provides a high frequency forcing through the induced vortex shedding, unveiling the rod mystery. To conclude, if many varied experiments exist on cavity flow control only a few numerical
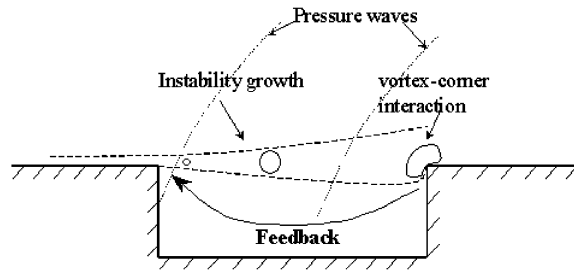
Fig. 1. Schematic view of the self-sustained pressure oscillations.

simulations have been carried out. Rona (2004) studied streamwise air injection by solving the bidimensional RANS equations with a $k-\omega$ closure, and Rizzetta and Visbal (2003) proposed high frequency mass injection for supersonic outer flows.

In this paper, we focus on two passive control strategies: the rod-in-crossflow and the flat-top spoiler. Experiments have been carried out by QinetiQ using a generic cavity rig in the ARA Bedford and DERA Bedford wind tunnels. The data consists of pressure time histories measured on the floor of the cavity using Kulite transducers along the centreline of the rig, which did not coincide with the centreline of the cavity itself. Despite prominent wind-tunnel tests, experiments did not provide clear explanations on the physics induced. Here, we aim at simulating the subsonic flow ($M_\infty = 0.85$) over a cavity of length/depth ratio equal to 5, with and without the noise suppression devices, and enhance the available database, with many measurements of the pressure time histories and the mean field.

The paper is organized as follows: first, we describe the studied experimental configuration with and without control devices and the corresponding meshes used for computation. Then we briefly comment the numerical strategy of our code. The numerical results are then exposed: the case without control is firstly shown to validate our approach, and eventually we assess and comment the efficiency of the two different control devices. Finally, conclusions are drawn in the last section.

2. Configuration and numerical parameters

2.1. Basic configuration

The computational set-up duplicates the experimental one, which deals with a rectangular open cavity of length over depth ratio $L/D = 5$. Its length L is equal to 508 mm (20 in), the width W, and the depth D are equal to 101.6 mm (4 in). The incoming flow is at Mach number of $M_\infty = 0.85$, obtained from an isentropic state characterized by $T_i = 301$ K and $p_i = 99\,540$ Pa, corresponding to an upstream velocity $u_\infty = 276$ m/s, and a Reynolds number $Re_L \simeq 7 \times 10^6$.

The unstructured meshes have been constructed with an in-house code, using tetrahedra elements. Three different meshes have been used for a mesh-refining effect on the non-controlled case. Then, the rod with wake has been inserted in the finest mesh, while the spoiler is simply obtained by removing elements. The parameters for the different grids used are summarized in Table 1.

The experimental sampling time is about 3.4 s with a sampling rate of 6 kHz, whereas numerically 0.3 s are computed with an integration time step of 10^{-5} s, i.e. 100 kHz. This time step, along with an efficient implicit time-integration strategy, provides maximum CFL numbers up to 800 approximately, depending on the meshes. Eventually, note that this case is now a benchmark provided by AGARD (Henshaw, 2000).

2.2. Flow-control devices

This paper investigates two different passive acoustic suppression strategies: the rod-in-crossflow and the flat-top spoiler. These devices are included in the QinetiQ database. Nevertheless, whereas the uncontrolled case is an open dataset for CFD validation, the suppression results were still confidential by the time the computations were performed, so that the configurations may slightly differ. Anyway, given a good experiment–computation concordance, we will use this database in a qualitative way, because we believe it is relevant to assess our computations. Table 2 synthesizes the important parameters of the control devices, which are sketched in Fig. 2.

Table 1
Grid parameters of the different computational set-ups

	Coarse mesh M1	Int. mesh M2	Fine mesh M3	Rod	Spoiler
Number of nodes	5×10^5	10^6	1.5×10^6	2.5×10^6	1.5×10^6
Number of elts	3×10^6	6×10^6	9×10^6	12×10^6	9×10^6
Domain size $(\times D)$	$(13, 4, 10)$	$(13, 4, 10)$	$(20, 6, 10)$	$(20, 6, 10)$	$(20, 6, 10)$

Table 2
Geometry of computational configurations

Spoiler		Rod	
H (mm)	11.34	ϕ (mm)	7.56
d (mm)	3.78	d (mm)	7.56
l (mm)	7.56	h (mm)	3.78
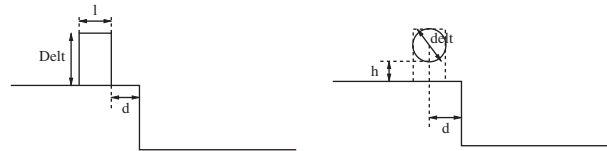
Fig. 2. Sketch of flow-control devices.

3. Numerical method

The code used for the study is AETHER, developed at Dassault-Aviation. It relies on a semi-discrete Galerkin/least-squares formulation of the symmetrized compressible Navier–Stokes equations (see Hughes et al., 1986) for a description of entropy variables used to symmetrize the equations). The time integration is carried out using an implicit second order backward difference scheme and piecewise linear elements are used for space discretization. A detailed description of this method applied to LES is found in Chalot et al. (1998) and Levasseur et al. (2005, 2006). A selective Smagorinsky is used to perform Large Eddy Simulation.

4. Validation on the cavity flow without control

The relevance of Large Eddy Simulation for compressible cavity flows has already been demonstrated, in particular in Larchevêque et al. (2003, 2004). In this section, we assess the ability of our numerical formulation to correctly compute the flow over an open cavity without control and to predict the Rossiter modes in both frequency and levels.

4.1. Grid convergence

We first analyse a grid refinement effect. Elements are mainly added inside the enclosure between M1 and M2 meshes. The influence of the domain size is also investigated between M2 and M3 meshes (see Table 1). Table 3 gives the position of the four Rossiter modes computed on three meshes at the bottom of the recess, compared with the experimental measurements (Kulite K20–K29) and the values obtained by Rossiter's formula (1). As advocated by Larchevêque et al. (2003) the value $\kappa = 0.57$ and $\gamma(L/D) = 0.29$ are used in Eq. (1). Note that the Rossiter mode frequencies are almost independent from the streamwise location, the error being of about ± 5 Hz. We observe very satisfactory agreement with the experiments, especially on mesh 3, considering that the maximum frequency precision is around 12 Hz, settled by the parameters of the signal processing algorithms. Only slight differences appear on the first mode, which is directly linked with the computational sampling time.

Table 3
Frequency of pressure spectrum peaks

Peak number	1	2	3	4
Rossiter's formula	148 Hz	357 Hz	566 Hz	775 Hz
Experiments	144 Hz	353 Hz	594 Hz	813 Hz
Mesh 1	136 Hz	462 Hz	625 Hz	873 Hz
Mesh 2	160 Hz	412 Hz	625 Hz	880 Hz
Mesh 3	108 Hz	362 Hz	594 Hz	838 Hz

Frequency precision ∼12 Hz
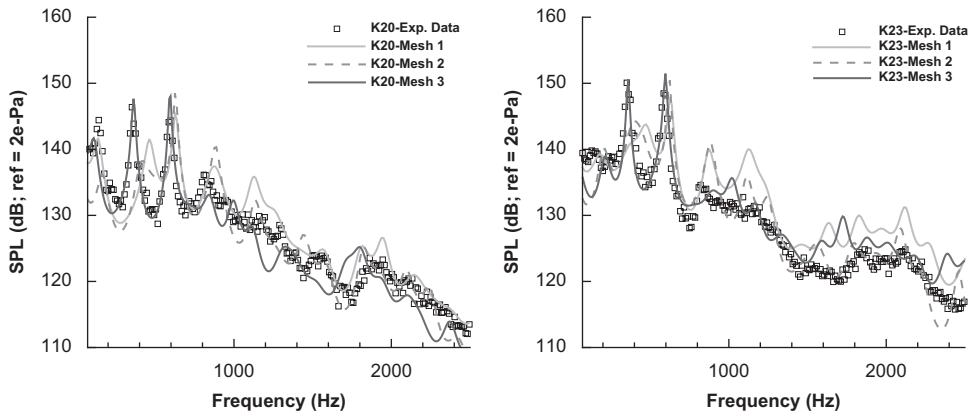
The subgrid model for computation is selective Smagorinsky.

Fig. 3. Grid convergence on the pressure spectra on the floor of the cavity (SPL) at two different positions: K20 and K23.

Fig. 3 compares the computed pressure power spectra with experimental data at two probe locations. The experimental spectra are obtained by fast Fourier transform on 4096-blocks, whereas the LES spectra are obtained thanks to Burg spectrum-estimator algorithm (Burg, 1978). This latter algorithm provides accurate spectra with resolved peaks and smooth base noise level and remains efficient for short-time samples (computed physical time is about 10 times shorter than experimental sampling time). The spectra are shown in sound pressure level (SPL) with a reference pressure at 2×10^{-5} Pa.

There is little difference between M1 and M2 computations. Both quite miss the second peak whereas it is very well predicted by M3 computation. The latter provides very accurate spectra, and captures Rossiter modes in terms of frequency and level.

5. Assessment of the pressure-fluctuation control devices

In this section, we will compare the efficiency and mechanisms of two passive acoustic oscillation suppression devices, namely the rod-in-crossflow and the spoiler.

5.1. Analysis of the mean field

First of all, the computed mean profiles are plotted in Figs. 4 to 7 at different streamwise locations. Streamwise and vertical velocity, turbulent kinetic energy and cross Reynolds stress are displayed. At location $x = 0$, i.e. just beyond the suppression device, the wakes of the rod and the spoiler clearly appear, with a large deficit of streamwise velocity and turbulent kinetic energy. Then, along the cavity centreline, we can see the deflection effect of both devices which is about of the same order of magnitude, together with a thickening of the mixing layer.
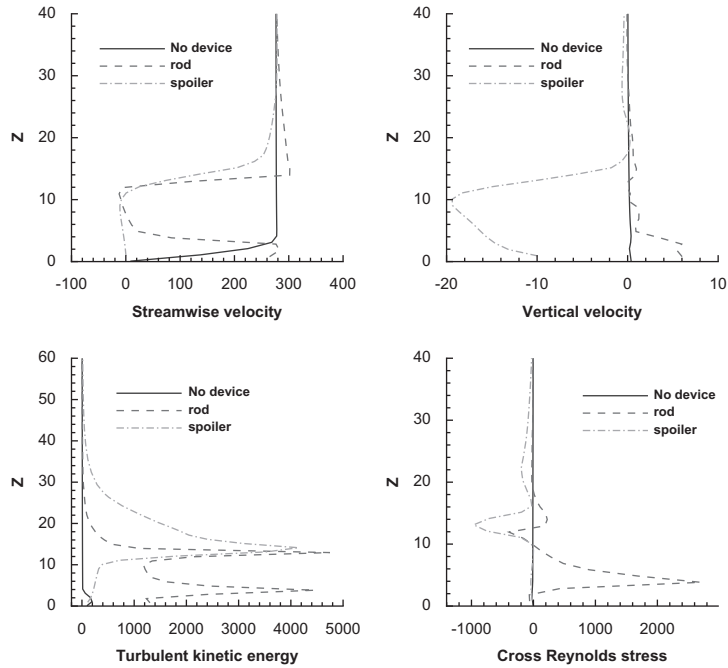
Fig. 4. Mean profile of streamwise and vertical velocity, turbulent kinetic energy, and cross Reynolds stress $u'w'$ in the mid-plane $y = 0$ at $x = 0$.
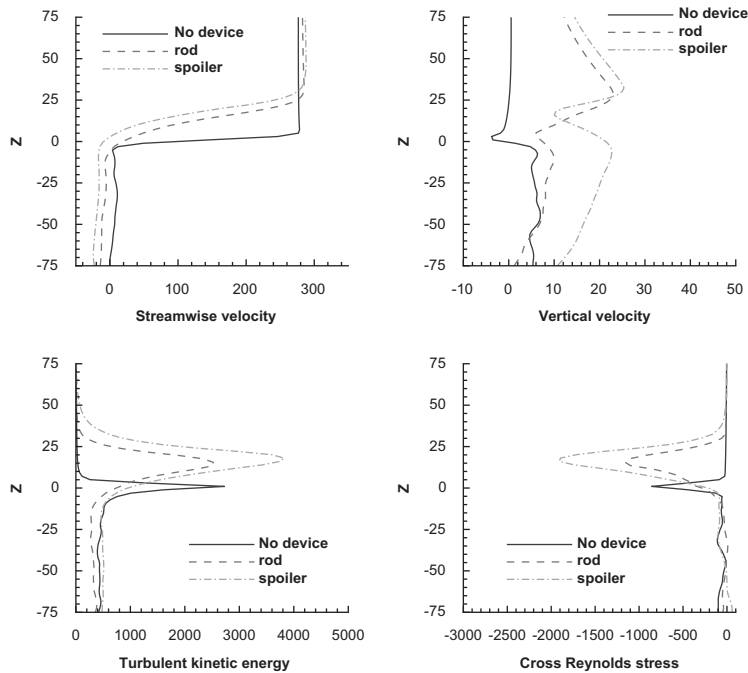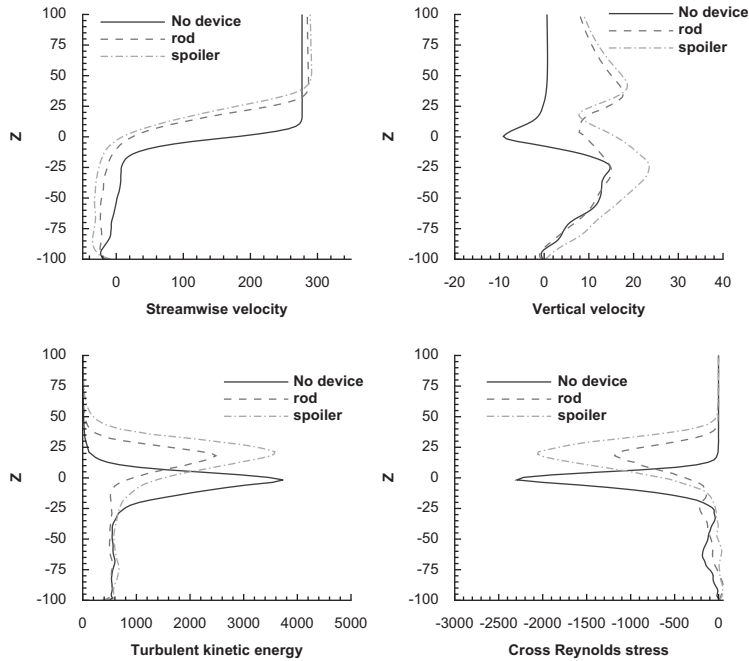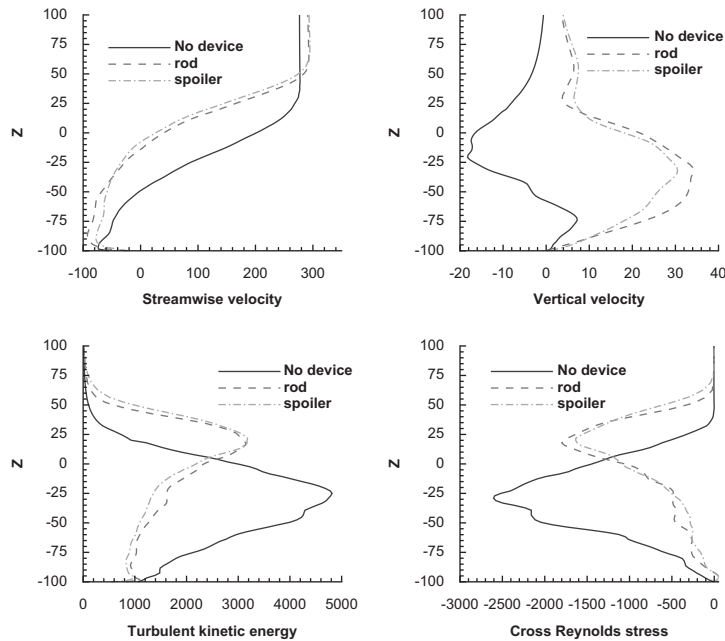

Fig. 5. Mean profile of streamwise and vertical velocity, turbulent kinetic energy, and cross Reynolds stress $u'w'$ in the mid-plane $y = 0$ at $x = L/10$.

Besides, compared with the spoiler, the rod-in-crossflow seems to generate less turbulence. Nevertheless, beyond $x = L/4$ the mixing layer contains more turbulent kinetic energy in the case without control. Therefore, we can summarize the effect of the suppression devices, which are quite similar so far, as follows: an upward translation

Fig. 6. Mean profile of streamwise and vertical velocity, turbulent kinetic energy, and cross Reynolds stress $u'w'$ in the mid-plane $y = 0$ at $x = L/5$.

Fig. 7. Mean profile of streamwise and vertical velocity, turbulent kinetic energy, and cross Reynolds stress $u'w'$ in the mid-plane $y = 0$ at $x = L/2$.

and enhancement of the mixing layer, a reduction of the mean kinetic energy as well as the downstream turbulent kinetic energy. Hence, at first sight the suppression features are due to the deflection effect and the reduction of energy.

5.1.1. Pressure on the floor of the cavity

We now analyse the effect of the control devices on the aerodynamic load experienced by the bay. Despite the control, the Rossiter modes are still visible at the bottom of the recess. The peaks are not as sharp as before and the streamwise modulation is important. Note that depending on the location, certain tones are almost entirely inhibited. For instance, remark that the fourth peak has totally vanished with the rod control. Table 4 gives the frequency position of each peak, when available, and Figs. 8 to 11 show the SPL spectra. Note that experimental and computational results cannot perfectly agree since the experimental configuration does not exactly match the numerical ones. Besides, equipment problems caused corruptions of certain rod-experiment data, and a few kulite positions are thus unavailable. Nonetheless, we believe that the comparisons still remain relevant, qualitatively.

Table 4
Frequency of pressure spectra peaks for the three different configurations

Peak number	1	2	3	4
Rossiter's formula	148 Hz	357 Hz	566 Hz	775 Hz
Exp without device	144 Hz	353 Hz	594 Hz	813 Hz
LES without device	108 Hz	362 Hz	594 Hz	838 Hz
LES with rod	113 Hz	376 Hz	609 Hz	–
Exp with rod	–	367 Hz	574 Hz	–
LES with spoiler	122 Hz	376 Hz	609 Hz	881 Hz
Exp with spoiler	–	380 Hz	613 Hz	876 Hz

Frequency precision ~12 Hz

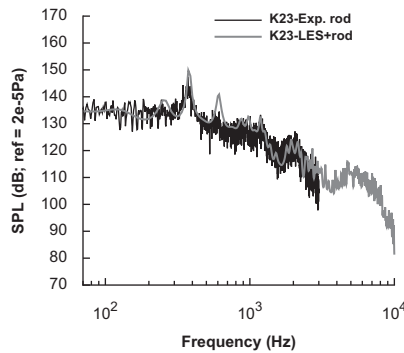The subgrid model for computation is selective Smagorinsky.

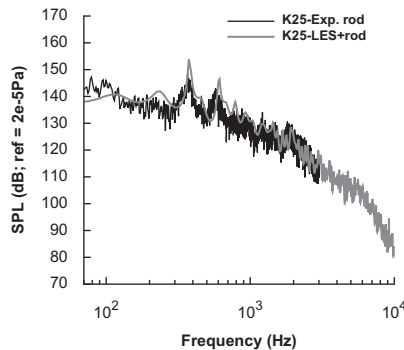Fig. 8. SPL pressure power spectra—LES versus experiment-rod case—K23.

Fig. 9. SPL pressure power spectra—LES versus experiment-rod case—K25.
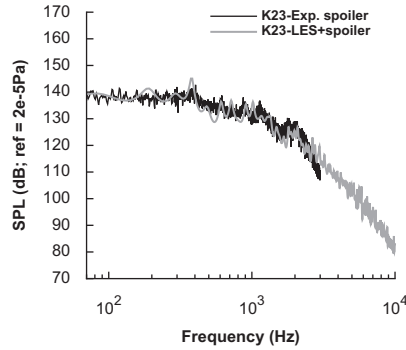
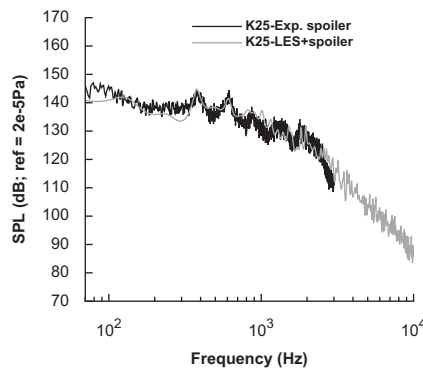Fig. 10. SPL pressure power spectra—LES versus experiment-spoiler case—K23.

Fig. 11. SPL pressure power spectra—LES versus experiment-spoiler case—K25.

Indeed, in spite of the slight differences in the tested configurations, the computations are in quite good agreement with experiment. The Rossiter tones are correctly captured in terms of frequency, but the second peak is generally greatly overpredicted, especially when controlling with the rod. Note that this second peak already caught out the previous computations performed on the coarse meshes, without control devices (see Section 4). On the other hand, it is interesting to see that the LES-with-rod computation recovers the trail of the Von Karman instability induced by the rod, all along the first half of the cavity. The corresponding spectrum, Fig. 8, presents a hump for a frequency of about 5500 Hz. Assuming a Strouhal number of 0.2 this frequency corresponds to an upstream velocity of 210 m/s, which is coherent while keeping in mind the rod is located in the outer part of the boundary layer.

Figs. 12 and 13 show the comparison of the computed pressure spectra for the three different configurations, namely the cavity without control, and the cavity controlled by the rod and the spoiler. It underlines the reduction of the pressure level, and the frequential overlapping of the remaining tones with the original Rossiter modes, obtained with both control devices. Moreover, differences in their proper mechanisms begin to appear between the rod and the spoiler. Firstly, the impact of the Karman vortices on the total pressure levels does not appear negligible. This point will be discussed in the following. Besides, the spoiler seems to reduce the amplitude of pressure peaks, as much as almost removing certain tones, while maintaining a high base-level. On the contrary, the mechanism of production of the Rossiter modes seems more present with the rod, since the peaks appear rather sharply, whereas the base-level has diminished.

The reduction effect is examined with emphasis on the Rossiter modes in Fig. 14, displaying the pressure energy contained in each of the four modes. We can observe an important gain on the third peak, whereas the reduction on the second Rossiter tone is maybe not as large as expected, as it was foreseeable on the spectra. Figs. 8 to 11 showing an overprediction of the amplitude of this peak.

Fig. 15(a) shows the streamwise evolution of band-integrated SPL corresponding to the primary Karman instability frequency for both suppression devices. One can see the influence of this instability caused by the rod over half the cavity. This is confirmed plotting the pressure fluctuations related to Rossiter mode frequency band normalized using the local total pressure fluctuation value. Indeed, when using the rod, the Rossiter modes contribution is lower
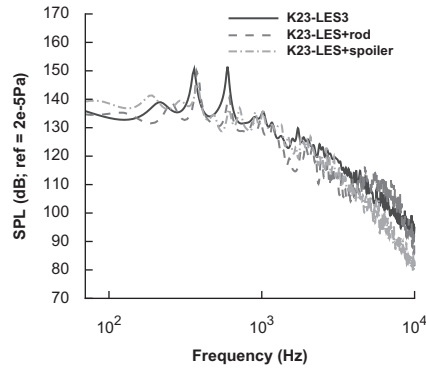
Fig. 12. Computed SPL pressure power spectra—K23.
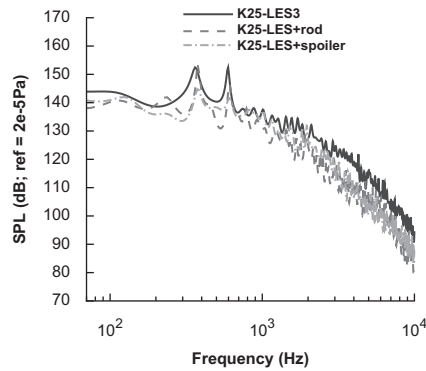
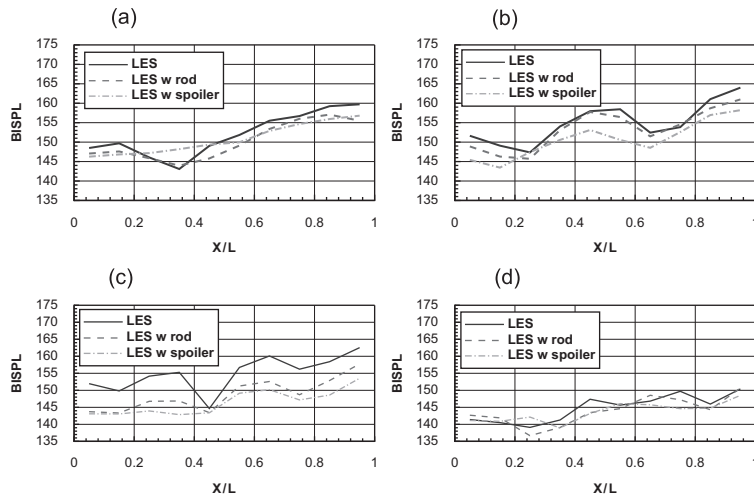

Fig. 13. Computed SPL pressure power spectra—K25.

Fig. 14. Streamwise evolution of band-integrated pressure fluctuations levels in BISPL: (a) 1st mode, (b) 2nd mode, (c) 3rd mode, and (d) 4th mode. Comparison of devices efficiency with numerical data.

upstream, at a location corresponding to the increase of the pressure fluctuations due to Karman instability. Besides, one can note a drop in the Rossiter modes contribution around $x/D = 4$. This has already been highlighted numerically by Larchevêque et al. (2004) and experimentally on a similar configuration by Heller and Bliss (1975). This drop is a
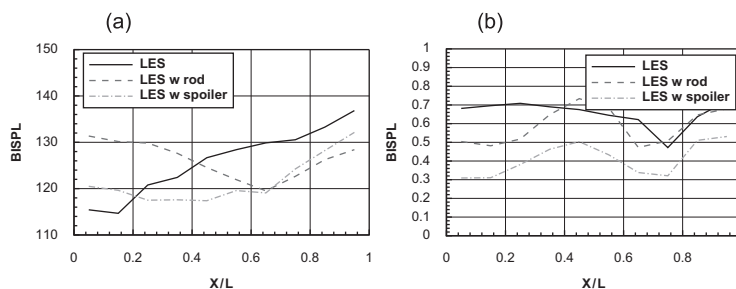
Fig. 15. Streamwise evolution of band-integrated sound pressure levels of: the Karman instability on the floor of the cavity, 5200–5800 Hz (left), and the Rossiter modes frequency band normalized by the total pressure fluctuations (right).

consequence of the existence of a node for modes 2 and 3 at this location. Furthermore, the Rossiter modes contribute for a constant value of 70% approximatively, without control, whereas their contribution varies between 30% and 50% with the spoiler, and between 50% and 70% with the rod. This confirms again that the spoiler tends to diminish the influence of the Rossiter modes, while the rod rather affects the pressure base-level than the single tones.

6. Conclusions

Numerical simulations of the control of cavity flows have been carried out to enhance experimental database. The influences of a rod and a spoiler located in the upstream boundary layer have been compared in order to find the device most likely to lower the aerodynamic loads inside the enclosure. Despite a different suppression mechanism, the average reduction of the total pressure level is quite similar for both devices, leading to an average 3–4 dB reduction. However, differences between the physics induced by the rod and the spoiler have been pointed out. The spoiler lowers the Rossiter modes contribution in the pressure oscillations, while the rod diminishes the global pressure level maintaining strong peaks. Future works will attempt in particular to unveil possible scale coupling between the rod wake and the mixing layer intrinsic instabilities.

Acknowledgements

References

Arunajatesan, S., Sinha, N., 2001. Unsteady RANS-LES simulations of cavity flowfields. AIAA paper 2001-0516.

Avital, E.J., 2001. Direct and large eddy simulations of compressible open cavity flows. In: Geurts, B.J., Friedrich, R. (Eds.), Direct and Large-Eddy Simulations IV. Kluwer Academic Publishers, Dordrecht, pp. 213–220.

Burg, J.P., 1978. Maximum entropy spectral analysis. In: Childers, D.G. (Ed.), Modern Spectrum Analysis. IEEE Press, New York, pp. 42–48.

Cattafesta, L., Williams, D., Rowley, C., Alvi, F., 2003. Review of active control of flow-induced cavity resonance. AIAA paper 2003-3567.

Cattafesta, L.N., Garg, S., Choudhari, M., Li, F., 1997. Active control of flow-induced cavity resonance. AIAA paper 97-1804.

Chalot, F., Marquez, B., Ravachol, M., Ducros, F., Nicoud, F., Poinsot, T., 1998. A consistent finite element approach to large Eddy simulation. AIAA paper 98-2652.

Dubief, Y., 2000. Simulation des grandes echelles de la turbulence de la region de proche paroi et des ecoulements decolles. Ph.D. Thesis, Institut National Polytechnique Grenoble (in French).

Forestier, N., Jacquin, L., Geffroy, P., 2003. The mixing layer over a deep cavity at high-subsonic speed. Journal of Fluid Mechanics 475, 101–145.

Gharib, M., Roshko, A., 1987. The effect of flow oscillations on cavity drag. Journal of Fluid Mechanics 177, 501–530.

Gloerfelt, X., Bogey, C., Bailly, C., Juve, D., 2002. Aerodynamic noise induced by laminar and turbulent boundary layers over rectangular cavities. AIAA paper 2002-2476.

Heller, H.H., Bliss, D.B., 1975. The physical mechanism of flow-induced pressure fluctuations in cavities and concepts for their suppression. AIAA paper 75-491.

Henshaw, C., 2000. M219 Cavity case. In: Verification and Validation Data for Computation Unsteady Aerodynamics, RTO-TR-26, AC/323(AVTTP/19).

Hughes, T.J.R., Franca, L.P., Mallet, M., 1986. A new finite element formulation for computational fluid dynamics: I. Symmetric forms of the compressible Euler and Navier–Stokes equations and the second law of thermodynamics. Computer Methods in Applied Mechanics and Engineering 54, 223–234.

Knisley, C., Rockwell, D., 1987. Self-sustained low frequency components in an impinging flows over cavities—a survey. AIAA paper 87-0166.

Labbe, O., Sagaut, P., Montreuil, E., 2002. Large-eddy simulation of heat transfer over a backward-facing step. Numerical Heat Transfer Part A—Applications 42, 73–90.

Larchevêque, L., Sagaut, P., Mary, I., Labbe, O., 2003. Large-eddy simulation of a compressible flow past a deep cavity. Physics of Fluids 15, 193–210.

Larchevêque, L., Sagaut, P., Lê, T.H., Comte, P., 2004. Large-eddy simulation of a compressible flow in a three-dimensional open cavity at high Reynolds number. Journal of Fluid Mechanics 516, 265–301.

Larchevêque, L., Sagaut, P., Labbe, O., 2007. Large-eddy simulation of a subsonic cavity flow including asymmetric effects. Journal of Fluid Mechanics 577, 105–126.

Levasseur, V., Sagaut, P., Chalot, F., Davroux, A., 2005. An entropy-variable-based VMS/GLS method for the simulation of compressible flows on unstructured grids. Computer Methods in Applied Mechanics and Engineering 195, 1154–1179.

Levasseur, V., Sagaut, P., Mallet, M., 2006. Subgrid models for large-eddy simulation using unstructured grids in a stabilized finite element framework. Journal of Turbulence 7, N28.

Lin, J.C., Rockwell, D., 2001. Organized oscillations of initially turbulent flow past a cavity. AIAA Journal 39 (6), 1139–1151.

Manoha, E., Troff, B., Sagaut, P., 2000. Trailing-edge noise prediction using large-eddy simulation and acoustic analogy. AIAA Journal 38, 575–583.

Meyers, J., Sagaut, P., Geurts, B.J., 2006. Optimal model parameters for multi-objective large-eddy simulations. Physics of Fluids 18, 095103.

Oshkai, P., Geveci, M., Rockwell, D., Pollack, M., 2005. Imaging of acoustically coupled oscillations due to flow past a shallow cavity: effect of cavity length scale. Journal of Fluids and Structures 20, 277–308.

Quemere, P., Sagaut, P., Couailler, V., 2001. A new multi-domain/multi-resolution method for large-eddy simulation. International Journal for Numerical Methods in Fluids 36, 391–416.

Raverdy, B., Mary, I., Sagaut, P., 2003. High-resolution large-eddy simulation of flow around a low-pressure turbine blade. AIAA Journal 41, 390–397.

Rizzetta, D.P., Visbal, M.R., 2003. Large-eddy simulation of supersonic cavity flow fields including flow control. AIAA Journal 41 (8), 1452–1562.

Rockwell, D., Lin, J.C., Oshkai, P., Reiss, M., Polack, M., 2003. Shallow cavity flow tone experiments: onset of locked-on states. Journal of Fluids and Structures 17, 381–414.

Rona, A., 2004. Control of transonic cavity flow instability by streamwise air injection, AIAA paper 2004-682.

Rossiter, J.E., 1964. Wind-tunnel experiments on the flow over rectangular cavities at subsonic and transonic speeds. Reports and Memoranda 3438, Aeronautical Research Council.

Sagaut, P., 2005. Large-Eddy Simulation for Incompressible Flows, third ed. Springer, Berlin.

Sagaut, P., Deck, S., Terracol, M., 2006. Multiscale and Multiresolution Approaches in Turbulence. Imperial College Press.

Sarohia, V., 1975. Experimental and analytical investigation of oscillations in flows over cavities. Ph.D. Thesis, California Institute of Technology.

Shieh, C.M., Morris, P.J., 2000. Parallel computational aeroacoustic simulation of turbulent subsonic cavity flow. AIAA paper 2000-1914.

Sinha, N., Dash, S.M., Chidambaram, N., Finlay, D., 1998. A perspective on the simulation of cavity aeroacoustics. AIAA paper 98-0286.

Stanek, M.J., Raman, G., Kibens, V., Ross, J.A., Odedra, J., Peto, J.W., 2000. Control of cavity resonance through very high frequency forcing. AIAA paper 2000-1905.

Stanek, M.J., Raman, G., Kibens, V., Ross, J.A., Odedra, J., Peto, J.W., 2001. Suppression of cavity resonance using high frequency forcing—the characteristics signature of effective devices. AIAA paper 2001-2128.

Stanek, M.J., Raman, G., Ross, J.A., Odedra, J., Peto, J.W., Alvi, F., Kibens, V., 2002. High frequency acoustic suppression—the role of mass flow, the notion of superposition and the role of inviscid instability—a new model (part II). AIAA paper 2002-2404.

Stanek, M.J., Ross, J.A., Odedra, J., Peto, J.W., 2003. High frequency acoustic suppression—the mystery of the rod-in-crossflow revealed. AIAA paper 2003-0007.

Terracol, M., Sagaut, P., Basdevant, C., 2001. A multilevel algorithm for large-eddy simulation of turbulent compressible flows. Journal of Computational Physics 167, 439–474.

Ziada, S., Ng, H., Blake, C.E., 2003. Flow excited resonance of a confined shallow cavity in low Mach number flow and its control. Journal of Fluids and Structures 18, 79–92.